

Mössbauer Evidence for Antisymmetric Exchange in a Diferric Synthetic Complex and Diferric Methane Monooxygenase

Karl E. Kauffmann,[†] Codrina V. Popescu,[†] Yanhong Dong,[‡] John D. Lipscomb,[§] Lawrence Que, Jr.,[‡] and Eckard Münck^{*,†}

Contribution from the Department of Chemistry, Carnegie Mellon University, Pittsburgh, Pennsylvania 15213, Department of Chemistry, University of Minnesota, Minneapolis, Minnesota 55455, and Department of Biochemistry, University of Minnesota, Minneapolis, Minnesota 55455

Received March 30, 1998

Abstract: The dinuclear iron cluster of the oxidized hydroxylase component of methane monooxygenase (MMOH) contains two antiferromagnetically coupled high-spin ferric ions ($\neq JS_A \cdot S_B$, $S_A = S_B = 5/2$, $J = 15 \text{ cm}^{-1}$). Previous Mössbauer studies revealed that the electronic ground state of the cluster contains a paramagnetic admixture; this is manifested in magnetic hyperfine splittings that are larger by about 10% than those attributable to the applied magnetic field. This observation cannot be explained by anisotropic Zeeman interactions, zero-field splittings, or anisotropic exchange. Here we report Mössbauer and magnetization studies of the (μ -phenoxo)bis(μ -carboxylato)diiron(III) complex, $[\text{Fe}_2(\text{HXTA})(\text{O}_2\text{CCH}_3)_2]^-$, **1**; HXTA = *N,N'*-(2-hydroxy-5-methyl-1,3-xylylene)bis(*N*-carboxymethylglycine). Like MMOH, complex **1** contains a pair of antiferromagnetically coupled high-spin ferric ions (our magnetization data yield $J = 20 \pm 2 \text{ cm}^{-1}$), and its 4.2 K Mössbauer spectra also exhibit increased magnetic splittings. Studies of the $\text{Ga}^{\text{III}}\text{Fe}^{\text{III}}$ analogue of **1** revealed no unusual properties of the high-spin Fe(III) site, suggesting that the increased magnetic splittings are attributes of the pair rather than properties of the local sites. The Mössbauer spectra of **1** recorded in parallel applied field exhibit nuclear $\Delta m = 0$ transitions, indicating the presence of an interaction that produces at each iron site spin expectation values in directions perpendicular to the applied field. Analysis of the data of **1** shows that the unusual spectral features of the complex, and by extension those of MMOH, reflect the presence of antisymmetric exchange, $\mathbf{d} \cdot (\mathbf{S}_A \times \mathbf{S}_B)$; we obtained $|\mathbf{d}| = 2.2 \pm 0.7 \text{ cm}^{-1}$ for complex **1** and $|\mathbf{d}| \approx 1.5 \text{ cm}^{-1}$ for MMOH. This study shows that Mössbauer spectroscopy can be a sensitive tool for determining antisymmetric exchange interactions.

Introduction

For the past decade we have studied in our laboratories the diiron proteins methane monooxygenase hydroxylase (MMOH) and ribonucleotide reductase as well as a variety of synthetic diiron complexes designed to model structural and electronic features of the clusters observed in the biological systems.^{1–4} In the diferric state, the metal centers of the two enzymes contain antiferromagnetically ($JS_A \cdot S_B$) coupled pairs of high-spin ($S_A = S_B = 5/2$) Fe(III) ions, yielding a ground state with total spin $S = 0$. From a magnetochemical point of view, the diferric clusters in MMOH and ribonucleotide reductase are quite distinct. The cluster in ribonucleotide reductase exhibits strong antiferromagnetic exchange ($J \approx 180 \text{ cm}^{-1}$)⁵ while that of

MMOH is weakly coupled ($J = 15 \text{ cm}^{-1}$).¹ EXAFS,⁶ resonance Raman,⁷ and X-ray crystallographic⁸ data for ribonucleotide reductase and comparison with structurally characterized model complexes have led to the conclusion that the iron sites of the dinuclear cluster are linked by a μ -oxo bridge.^{2,9} Observation of a smaller J value for MMOH had suggested that the bridging unit could not be a μ -oxo bridge.¹ Subsequent X-ray crystallographic studies of this enzyme have provided the structure shown in Scheme 1B for the diferric cluster.¹⁰

We previously observed that the 1.5 K Mössbauer spectra of diferric MMOH recorded in strong applied magnetic fields exhibited magnetic splittings approximately 10% larger than expected for a dinuclear system with a diamagnetic ground state.¹ These observations suggested that paramagnetic excited states were admixed into the ground state. Such admixtures may arise from anisotropic Zeeman interactions, $\sum_{i=A,B} \beta \mathbf{B} \cdot \mathbf{g}_i \cdot \mathbf{S}_i$, zero-field splittings (ZFS) of the two ferric sites, $\sum_{i=A,B} \mathbf{D}_i \cdot \mathbf{S}_i$ (D values for octahedral sites as in MMOH are typically

* To whom correspondence should be addressed: Phone 412-268-5058, FAX 412-268-1061, E-mail em40@andrew.cmu.edu.

[†] Carnegie Mellon University.

[‡] Department of Chemistry, University of Minnesota.

[§] Department of Biochemistry, University of Minnesota.

(1) Fox, B. G.; Hendrich, M. P.; Sureus, K. K.; Andersson, K. K.; Froland, W. A.; Lipscomb, J. D.; Münck, E. *J. Am. Chem. Soc.* **1993**, *115*, 3688–3701.

(2) Que, L., Jr.; True, A. E. *Prog. Inorg. Chem.* **1990**, *38*, 97–200.

(3) Kurtz, D. M. *Chem. Rev.* **1990**, *90*, 585–606.

(4) Wallar, J. B.; Lipscomb, J. D. *Chem. Rev.* **1996**, *96*, 2625–2657.

(5) Petersson, L.; Gräslund, A.; Ehrenberg, A.; Sjöberg, B.-M.; Reichard, P. *J. Biol. Chem.* **1980**, *255*, 6706–6712. Galli, C.; Atta, M.; Andersson, K. K.; Gräslund, A.; Brudvig, G. W. *J. Am. Chem. Soc.* **1995**, *117*, 740–746.

(6) Scarrow, R. C.; Maroney, M. J.; Palmer, S. M.; Roe, A. L.; Que, L., Jr.; Salowe, S. P.; Stubbe, J. *J. Am. Chem. Soc.* **1987**, *109*, 7857–7864.

(7) Sjöberg, B.-M.; Loehr, T. M.; Sanders-Loehr, J. *Biochemistry* **1982**, *21*, 96–102.

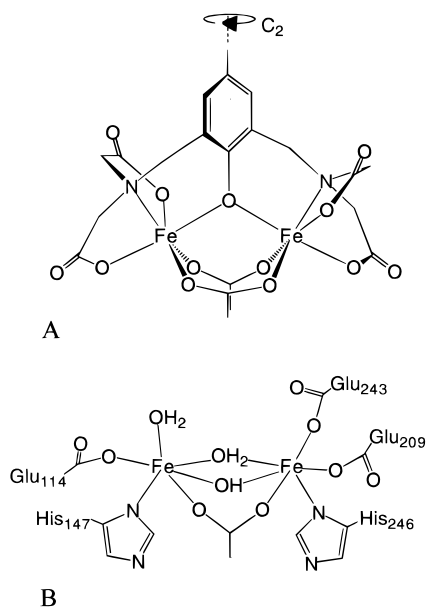
(8) (a) Nordlund, P.; Sjöberg, B.-M.; Eklund, H. *Nature* **1990**, *345*, 593.

(b) Nordlund, P.; Eklund, H. *J. Mol. Biol.* **1993**, *232*, 123.

(9) Sanders-Loehr, J. In *Iron Carriers and Iron Proteins*; Loehr, T. M., Ed.; VCH: New York, 1989; pp 373–466.

(10) Elango, N.; Radhakrishnan, R.; Froland, W. A.; Wallar, B. J.; Earhart, C. A.; Lipscomb, J. D.; Ohlendorf, D. H. *Protein Sci.* **1997**, *7*, 556–568.

Scheme 1



$|D_i| \leq 1 \text{ cm}^{-1}$), and anisotropic exchange, $\mathbf{S}_A \cdot \mathbf{D}_{AB} \cdot \mathbf{S}_B$. However, inclusion of these terms did not produce acceptable fits to the Mössbauer spectra.¹ In particular, the ZFS and anisotropic exchange interactions would produce effective fields at the ⁵⁷Fe nuclei that yield magnetic splittings that are smaller, rather than larger, than those expected for a diamagnetic compound. Furthermore, the \mathbf{g} tensors of high-spin Fe³⁺ sites are generally isotropic to within 1%, and thus no substantial mixing by the Zeeman term is expected.

In the course of a systematic study of dinuclear iron complexes, we have recorded the Mössbauer spectra of the (μ -phenoxo)bis(μ -carboxylato)diiron(III) complex, $[\text{Fe}^{\text{III}}\text{Fe}^{\text{III}}(\text{HXTA})(\text{O}_2\text{CCH}_3)_2]^-$ (HXTA = *N,N'*-(2-hydroxy-5-methyl-1,3-xylylene)bis(*N*-carboxymethylglycine)), **1**,¹¹ which yielded spectra with features similar to those observed for MMOH. As indicated in Scheme 1A, the two Fe sites of the HXTA complex are linked by a phenoxo oxygen and two acetate bridges. While the local sites of complex **1** have no symmetry element, the dimer has an (approximate) C_2 axis perpendicular to the internuclear axis. Because of the near site equivalence, the Mössbauer spectra of this complex are better resolved than those of MMOH, which allowed us to perform a detailed analysis of the data. This analysis suggests that the unexplained features of the low-temperature Mössbauer spectra of MMOH and of the HXTA complex have to be attributed to the presence of antisymmetric exchange. To our knowledge this paper presents the first evidence for antisymmetric exchange in a diferric complex.

The exchange interactions for a pair of paramagnetic ions with spins S_A and S_B can take the general form $H_{\text{ex}} = \mathbf{S}_A \cdot \mathbf{J}_{AB} \cdot \mathbf{S}_B$, where \mathbf{J}_{AB} is a 3×3 tensor that contains the relevant exchange parameters. \mathbf{J}_{AB} can be decomposed into a scalar J (generally the dominating term), a traceless symmetric tensor (\mathbf{D}_{AB}) describing *anisotropic* exchange, and an antisymmetric tensor.^{12,13} The *antisymmetric* exchange term can be written as $\mathbf{d} \cdot (\mathbf{S}_A \times \mathbf{S}_B)$ where \mathbf{d} is a pseudovector. The antisymmetric term was introduced by Dzyaloshinsky¹⁴ on symmetry grounds

(11) Murch, B. P.; Bradley, F. C.; Que, L., Jr. *J. Am. Chem. Soc.* **1986**, *108*, 5027–5028.

(12) Bencini, A.; Gatteschi, D. *Electron Paramagnetic Resonance of Exchange Coupled Systems*; Springer-Verlag: Berlin–Heidelberg, 1990.

(13) Moriya, T. In *Magnetism*; Rado, G. T., Suhl, H., Eds.; Academic Press Inc.: New York and London, 1963; pp 86–124.

(14) Dzyaloshinsky, I. *J. Phys. Chem. Solids* **1958**, *4*, 241–255.

and further explored by Moriya.¹⁵ Moriya formulated rules that specify the direction of \mathbf{d} for certain symmetries (suggesting for complex **1** that \mathbf{d} is in the plane perpendicular to the 2-fold axis). For systems with isolated orbital ground states, the Dzyaloshinsky–Moriya interaction arises in second order from an interplay between spin–orbit coupling and isotropic exchange. If the excited orbital states considered belong to the same spin multiplet as the ground-state orbitals, the antisymmetric interaction is of the order $(\Delta g/g)$ times an exchange integral J .¹⁵ It should be noted that J' is an exchange integral that contains a pathway involving excited orbital states and can differ, therefore, substantially from J ; however, for lack of information J is generally used for order of magnitude estimates.

Antisymmetric exchange has been frequently observed for magnetically ordered states of extended lattices where it gives rise to the well-studied phenomenon of spin canting.^{16,17} The term $\mathbf{J}\mathbf{S}_A \cdot \mathbf{S}_B$ leads to parallel or antiparallel alignment of \mathbf{S}_A and \mathbf{S}_B whereas the $\mathbf{d} \cdot (\mathbf{S}_A \times \mathbf{S}_B)$ term tends to orient the spins perpendicular to each other and perpendicular to \mathbf{d} (for a discussion, see Erdős¹⁸). For complex **1** we observed that an applied field to a polycrystalline sample induced a magnetic hyperfine field in a direction perpendicular to the applied field. This suggested to us a sizable $\mathbf{d} \cdot (\mathbf{S}_A \times \mathbf{S}_B)$ term.

Information about \mathbf{d} values for isolated complexes is scarce, and in part controversial. Nishimura and Date¹⁹ have explained anomalous \mathbf{g} value shifts of the Cr-trimer $[\text{Cr}_3\text{O}(\text{O}_2\text{CH}_2\text{CH}_3)_6(\text{H}_2\text{O})_3]\text{NO}_3 \cdot 2\text{H}_2\text{O}$ by assuming $d_z = 0.62 \text{ cm}^{-1}$. Rakitin et al.²⁰ have studied the X- and Q-band EPR spectra of the Fe-(III) acetate complex, $[\text{Fe}_3\text{O}(\text{O}_2\text{CCH}_2\text{CH}_3)_6(\text{H}_2\text{O})_3]\text{Cl} \cdot 5\text{H}_2\text{O}$, and deduced $|\mathbf{d}| = 1.4 \text{ cm}^{-1}$; this complex, like the systems studied here, contains high-spin Fe(III) sites. Lines and collaborators²¹ have fit magnetic susceptibility data of the tetrameric copper complex $[\text{Cu}_4\text{OCL}_6(\text{triphenylphosphine oxide})_4]$ by assuming a very large antisymmetric exchange interaction, $d_y \cong -28 \text{ cm}^{-1}$, between orbitally degenerate Cu²⁺ ions. Black and collaborators,²² however, on the basis of single-crystal EPR work, have derived for the same tetramer an energy level scheme, without invoking antisymmetric exchange, that is in gross conflict with the interpretation of the susceptibility data. Finally, Gutowski²³ on the basis of single-crystal EPR has concluded that the nearest neighbor Cr³⁺ pairs in the inverse spinel LiGa_5O_5 exhibit antisymmetric exchange with $d_x = 0.25 \text{ cm}^{-1}$.²⁴

Materials and Methods

$\text{Me}_4\text{N}[\text{Fe}_2(\text{HXTA})(\text{OAc})_2]$ (**1**) was prepared as described previously.¹¹ To a methanol solution of $\text{Fe}(\text{NO}_3)_3 \cdot 9\text{H}_2\text{O}$ (161.6 mg, 0.4 mmol, 2 mL) was added an aqueous solution of the trisodium salt of

(15) Moriya, T. *Phys. Rev.* **1960**, *120*, 91–98.

(16) Coffey, D.; Bedell, K. S.; Trugman, S. A. *Phys. Rev. B* **1990**, *42*, 6509–6514.

(17) Kahn, O. *Molecular Magnetism*; VCH Publishers: New York, 1993; Chapter 12.

(18) Erdős, P. *J. Phys. Chem. Solids* **1966**, *27*, 1705–1720.

(19) Nishimura, H.; Date, M. *J. Phys. Soc. Jpn.* **1985**, *54*, 395–399.

(20) Rakitin, Y. V.; Yablokov, Y. V.; Zelentsov, V. V. *J. Magn. Reson.* **1981**, *43*, 288–301.

(21) Lines, M. E.; Ginsberg, A. P.; Martin, R. L. *Phys. Rev. Lett.* **1972**, *28*, 684–687.

(22) Black, T. D.; Rubins, R. S.; De, D. K.; Dickinson, R. C.; Baker, W. A., Jr. *J. Chem. Phys.* **1984**, *80*, 4620–4624.

(23) Gutowski, M. *Phys. Rev. B* **1978**, *18*, 5984–5989.

(24) Gutowski has analyzed EPR data of the $S = 2$ excited state. The author points out that for a symmetric dimer with $S_1 = S_2 = 3/2$ this manifold does not exhibit a first-order splitting by zero-field splitting terms. However, the author neglects mixing of multiplets by these terms. Diagonalization of the Hamiltonian matrix of the $\text{Cr}^{3+}\text{Cr}^{3+}$ dimer shows that off-diagonal elements of the zero-field splitting interactions cause splittings of the $S = 2$ levels comparable to those attributed by Gutowski to antisymmetric exchange.

the dinucleating ligand (92.7 mg, 0.2 mmol, 1 mL), followed by a methanol solution of Et₃N (40.5 mg, 0.4 mmol, 2 mL). After 10 min of stirring, 270 mg of NaO₂CCH₃ and 120 mg of HO₂CCH₃ were added, followed by 43.8 mg of [Me₄N]Cl. Red crystals were obtained after 5 days by slow diffusion of acetone into the reaction solution. The crystals were collected by filtration and washed with ice-cold methanol, and dried in air. Crystals of a statistical mixture of FeFe, FeGa, and GaGa complexes were obtained following the procedure for **1** by using 0.2 mmol each of Ga(NO₃)₃·H₂O (54.8 mg) and Fe(NO₃)₃·9H₂O (80.8 mg) instead of 0.4 mmol of Fe(NO₃)₃·9H₂O.

Mössbauer spectra were recorded with a constant acceleration spectrometer. The samples were inserted into a Janis Research, Inc. dewar that housed a superconducting magnet and allowed the temperature of the sample to be controlled from 1.5 to 200 K. Magnetic fields up to 8.0 T were applied parallel to the observed γ -radiation. Isomer shifts are quoted relative to Fe metal at 298 K. To minimize texture effects (partial alignment by packing) and orientation of samples in the magnetic field, the polycrystalline samples were immersed in mineral oil and frozen.

For susceptibility measurements a polycrystalline sample of complex **1** was weighed and sealed into a gelatin capsule. Studies were performed on a MPMS SQUID susceptometer (Quantum Design). The instrument was calibrated with a palladium metal standard. Gelatin capsules were studied separately, and diamagnetic corrections for ligands were made by considering the single atom Pascal constants.

Results and Discussion

A suitable spin Hamiltonian for describing the low-lying spin levels of exchange coupled Fe³⁺–Fe³⁺ pairs in MMOH and the HXTA complex can be written as

$$H = H_e + H_{\text{hf}} \quad (1)$$

$$H_e = H_{\text{ex}} + \sum_{i=A,B} \beta \mathbf{S}_i \cdot \mathbf{g}_i \cdot \mathbf{H} + \sum_{i=A,B} \mathbf{S}_i \cdot \mathbf{D}_i \cdot \mathbf{S}_i \quad (2)$$

$$H_{\text{ex}} = J \mathbf{S}_A \cdot \mathbf{S}_B + \mathbf{S}_A \cdot \mathbf{D}_{AB} \cdot \mathbf{S}_B + \mathbf{d} \cdot (\mathbf{S}_A \times \mathbf{S}_B) \quad (3)$$

$$H_{\text{hf}} = \sum_{i=A,B} \{ A_0 \mathbf{S}_i \cdot \mathbf{I}_i - g_n \beta_n \mathbf{H} \cdot \mathbf{I}_i + H_Q(i) \} \quad (4)$$

$$H_Q = \sum_{i=A,B} \frac{eQV_{zz}(i)}{12} \left\{ 3I_z^2 - \frac{15}{4} + \eta(i)(I_x^2 - I_y^2) \right\} \quad (5)$$

The sums in eq 2 taken over sites A and B account for the Zeeman interactions and the zero-field splittings. Equation 4 describes the magnetic hyperfine interactions, the nuclear Zeeman interactions, and the electric quadrupole interactions; the latter is written in its principal axis form in eq 5. For high-spin Fe³⁺ the \mathbf{g}_i are isotropic to within about 1% and \mathbf{g} is close to the g factor of the free electron, $g_0 = 2.00$. Similarly, the magnetic hyperfine interactions of 6-coordinated high-spin Fe³⁺ sites are generally isotropic. Moreover, iron environments as those considered here typically yield zero-field splittings $|D_i| \leq 1 \text{ cm}^{-1}$.

Figure 1 shows zero-field Mössbauer spectra, recorded at 4.2 K, of polycrystalline complex **1** (A) and diferric MMOH (B). The HXTA complex exhibits one sharp quadrupole doublet with $\Delta E_Q = 0.59 \text{ mm/s}$ and $\delta = 0.48 \text{ mm/s}$. The observation of only one doublet is in accord with the X-ray data¹¹ which have revealed that complex **1** has two nearly equivalent Fe sites. The parameters for ΔE_Q and δ are consistent with high-spin Fe³⁺ sites in environments indicated in Scheme 1. The MMOH spectrum consists of a broadened doublet that reflects two cluster forms, each with two inequivalent Fe³⁺ sites (see caption of Figure 8). Figures 2A and 2B show the corresponding spectra

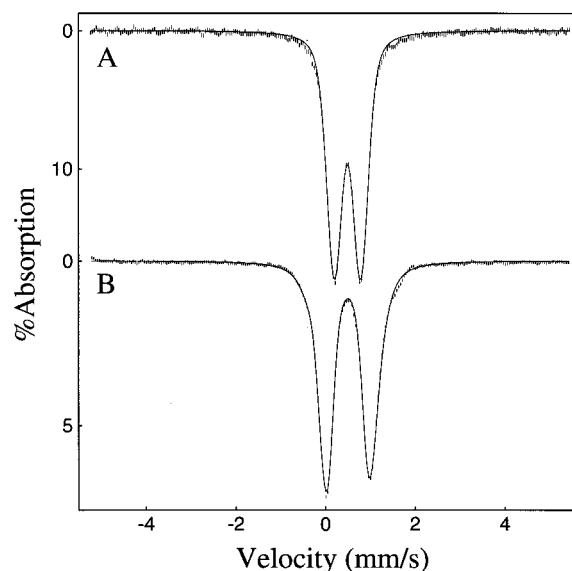


Figure 1. Mössbauer spectra of polycrystalline **1** (A) and diferric MMOH (B) recorded at 4.2 K in zero field. Solid lines are spectral simulations using the values for ΔE_Q and δ quoted in Table 1 for complex **1** and in the caption of Figure 8 for MMOH. For MMOH two cluster forms with 78% and 22% abundance were assumed. MMOH spectra shown in Figures 1, 2, and 8 are those of ref 1.

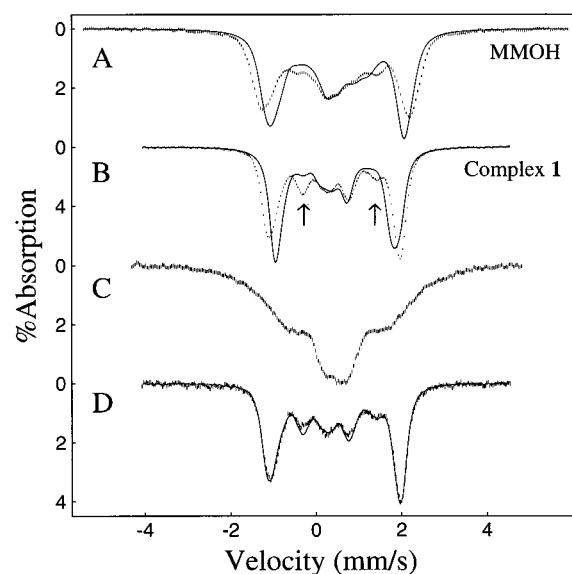


Figure 2. Spectra (8.0 T) of complex **1** and MMOH. (A) Frozen solution of diferric MMOH; polycrystalline sample of complex **1** at 4.2 K (B) and 30 K (C); in (D) the 4.2 K spectra of polycrystalline **1** (solid line) and complex **1** dissolved in methanol are compared. Solid lines in (A) and (B) are simulations based on eq 6 meant to illustrate how the spectra would appear if the ground states of the clusters were strictly diamagnetic.

recorded in 8.0 T fields applied parallel to the observed γ -radiation. Figure 2C shows an 8.0 T spectrum of complex **1** recorded at 30 K; this spectrum differs decidedly from that recorded at 4.2 K due to relaxational broadening, showing that low-lying spin multiplets are substantially populated at 30 K. In fact, population of excited states is apparent already at 10 K (not shown). These observations suggest that $J < 30 \text{ cm}^{-1}$.

Figure 3 shows SQUID magnetization data obtained for a polycrystalline sample of complex **1**. Analysis of the data (see caption and comments below) yields $J = 20 \text{ cm}^{-1}$ for the isotropic exchange coupling constant. Using this value for J , we have simulated the 4.2 K Mössbauer spectra of complex **1**

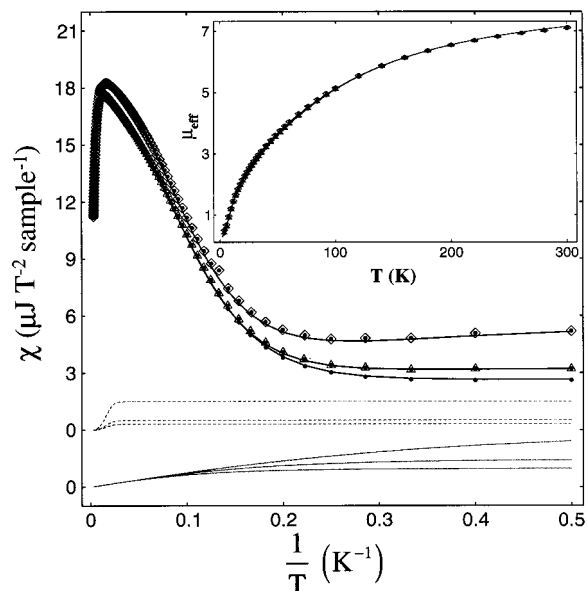


Figure 3. SQUID magnetization data of polycrystalline complex **1** obtained in applied fields of (\diamond) 1.0 T (upper curve), (\triangle) 3.0 T (middle), and (\bullet) 5.0 T (lower). The main plot shows χ vs $1/T$ and the inset depicts μ_{eff} vs T (for clarity, only every fourth data point has been plotted for the inset drawing). Susceptibility data have been adjusted with the diamagnetic correction $\chi_{\text{dia}} = -0.3 \mu\text{J T}^{-2} \text{ sample}^{-1}$. Solid lines drawn through the data are simulations based on eqs 2 and 3, using the parameters listed in Table 1; we used $D_{\text{AB}} = 0$, but the potential effect of the anisotropic exchange term is contained in D_{A} and D_{B} . Separately shown below the data are the contributions of a ferrous (solid lines, 0.8% of Fe) and a ferromagnetic (dashed, <0.3% of Fe) contaminant.

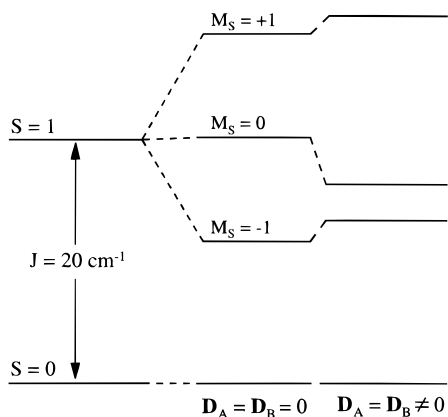


Figure 4. Lowest spin levels of the diferric clusters plotted to scale for $B = 8.0 \text{ T}$ and $J = 20 \text{ cm}^{-1}$.

by using the commonly employed electronic Hamiltonian

$$\begin{aligned}
 H &= J\mathbf{S}_{\text{A}} \cdot \mathbf{S}_{\text{B}} + g_0\beta\mathbf{B}(\mathbf{S}_{\text{A}} + \mathbf{S}_{\text{B}}) + H_{\text{hf}} \\
 &= J\{\mathbf{S}^2 - \mathbf{S}_{\text{A}}^2 - \mathbf{S}_{\text{B}}^2\}/2 + g_0\beta\mathbf{B} \cdot \mathbf{S} + H_{\text{hf}} \quad (6)
 \end{aligned}$$

where $\mathbf{S} = \mathbf{S}_{\text{A}} + \mathbf{S}_{\text{B}}$ is the system spin. Equation 6 yields a spin ladder whose $S = 0$ and 1 multiplets are shown in Figure 4. This predicts for $J = 20 \text{ cm}^{-1}$ a diamagnetic ground state for all applied fields employed in this study. The solid line in Figure 2B is a theoretical Mössbauer spectrum computed from eq 6. It can be seen that the magnetic splitting of the experimental spectrum is larger than that predicted by the theory; a similar observation applies to MMOH (Figure 2A). These observations imply that the electronic ground states of both clusters contain admixtures from excited states which produce

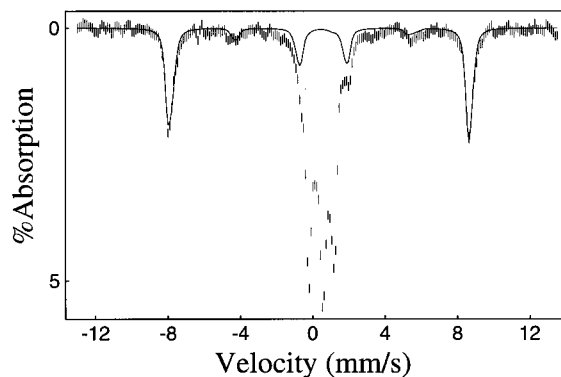


Figure 5. Mössbauer spectrum (3.0 T) of polycrystalline $\text{Ga}^{\text{III}}\text{Fe}^{\text{III}}$ HXTA complex, **2**, recorded at 1.5 K. The central region of the spectrum shows the contribution of complex **1**. The solid line is a spectral simulation for a monomeric high-spin ferric site for an $S = 5/2$ Hamiltonian, using parameters listed in Table 1 and a Lorentzian line width (FWHM), Γ , of 0.30 mm/s.

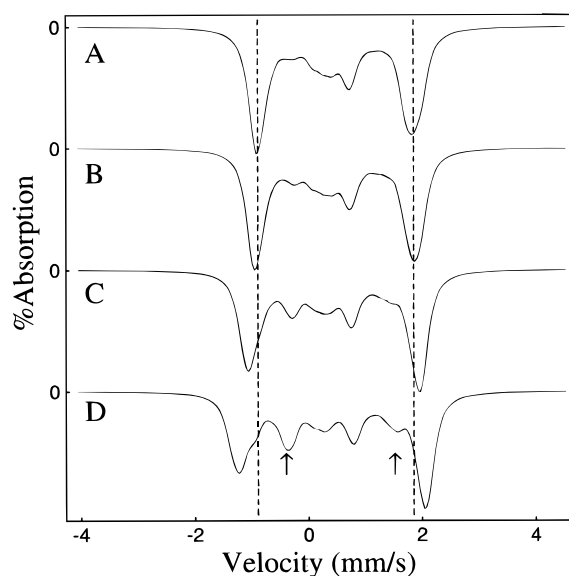


Figure 6. Calculated 8.0 T Mössbauer spectra illustrating the effect of the $\mathbf{d} \cdot (\mathbf{S}_{\text{A}} \times \mathbf{S}_{\text{B}})$ term. Spectra were computed with the parameters of Table 1 but varying d_z : (A) $d_z = 0$, (B) $d_z = 1 \text{ cm}^{-1}$, (C) $d_z = 2 \text{ cm}^{-1}$, and (D) $d_z = 3 \text{ cm}^{-1}$. The dashed lines mark the position of the outer bands for $d_z = 0$. $\Delta m = 0$ lines are indicated by arrows.

positive magnetic hyperfine fields that add to the applied field. A spectrum nearly identical²⁵ to that shown in Figure 2B was observed at 1.5 K, showing that the increased splitting does not result from population of a low-lying excited state. We have also recorded spectra at 4.2 K in applied fields of 3.0, 4.0, 6.0, and 7.0 T; all spectra exhibit a similar mismatch between observed splittings and those computed for a diamagnetic complex. Significantly, the experimental spectrum of Figure 2B exhibits two bands, marked by arrows, that are not properly described by the Hamiltonian of eq 6. To test whether any of the features can be attributed to solid-state effects, such as interactions between dimers, we have recorded Mössbauer spectra of the HXTA complex dissolved in acetonitrile. Comparison of the frozen solution spectrum of Figure 2D (hash-

(25) At 4.2 K the thermal population of the $M_S = -1$ level of the $S = 1$ multiplet is 1%. Assuming fast relaxation between just the $S = 0$ level and the $M_S = -1$ state explains the minor difference between the 1.5 and 4.2 K spectra. The assumption of fast relaxation between these two levels is not in conflict with the observation of intermediate relaxation rates at higher temperature because additional levels with different relaxation properties are involved.

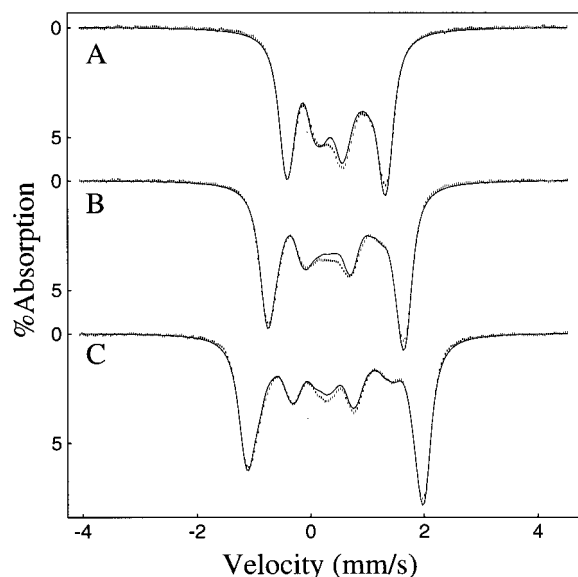


Figure 7. Mössbauer spectra of complex **1** recorded at 4.2 K in parallel applied fields of (A) 4.0, (B) 6.0, and (C) 8.0 T. The solid lines are spectral simulations based on eqs 1–5, using the parameters of Table 1 ($\Gamma = 0.28$ mm/s).

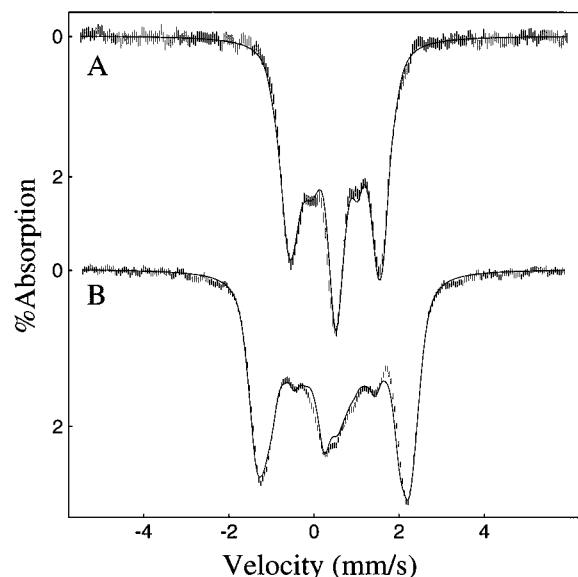


Figure 8. Mössbauer spectra of MMOH recorded at 4.2 K in applied fields of (A) 4.0 and (B) 8.0 T. The solid line is a spectral simulation assuming two cluster forms: 1 (78%) and 2 (22%). Cluster 1: $J = 15$ cm^{-1} , $g_0 = 2.0$, $d_y = 1.5$ cm^{-1} , $D_A = D_B = 0.5$ cm^{-1} , $(E/D)_A = (E/D)_B = 0$, $A_{\text{iso}}(A) = A_{\text{iso}}(B) = -30$ MHz, $\Delta E_Q(A) = -1.16$ mm/s, $\eta(A) = 1.0$, $\Delta E_Q(B) = -0.87$ mm/s, $\eta(B) = 0.2$, $\delta(A) = \delta(B) = 0.51$ mm/s, $\Gamma(A) = \Gamma(B) = 0.34$ mm/s. Cluster 2 (assuming $S = 0$): $\Delta E_Q(A) = 1.77$, $\eta(A) = 1$, $\Delta E_Q(B) = 0.82$ mm/s, $\eta(B) = 1$, $\delta(A) = \delta(B) = 0.48$ mm/s, $\Gamma(A) = \Gamma(B) \approx 0.3$ mm/s. The parameters, specifically ΔE_Q and δ values, used here for cluster 1 are in agreement with those reported by Fox et al.¹

marks) with that obtained for the polycrystalline sample (solid line in Figure 2D) shows that solid-state effects are not responsible for the peculiar features of the spectra of complex **1**.

The Zeeman and the zero-field splitting terms of eq 2 can admix a paramagnetic contribution into the ground singlet. However, as pointed out previously¹ for MMOH, inclusion of these terms cannot explain the experimental data. An even more compelling argument can be made for complex **1**. First, mixing by the Zeeman term is proportional to $\mathbf{g}_- = \mathbf{g}_A - \mathbf{g}_B$; see for

instance refs 12 and 26. For 6-coordinated high-spin Fe^{3+} in octahedral environments the ratio $\mathbf{g}_-/\mathbf{g}_{A,B}$ is expected to be about 0.01 or smaller and for complex **1** in particular the (approximate) C_2 axis implies that $\mathbf{g}_- = 0$. Moreover, a \mathbf{g}_- term would not produce a paramagnetic admixture that yields the correct internal field distribution. In particular, the bands marked by arrows in Figure 2B cannot be explained by inclusion of a \mathbf{g}_- term. Mixing of spin multiplets by the zero-field splitting terms of eq 2 is proportional to $\mathbf{D}_+ = \mathbf{D}_A + \mathbf{D}_B$. This term mixes $S = 2$ states into the ground singlet (the relevant matrix elements are listed in ref 12) and always produces *negative* magnetic hyperfine fields, i.e., the magnetic splittings would decrease rather than increase if such mixing would be significant. With the same arguments one can eliminate *anisotropic exchange*, $\mathbf{S}_A \cdot \mathbf{D}_{AB} \cdot \mathbf{S}_B$, because this interaction mixes the spin states similarly as the zero-field splittings.

Although we can rule out zero-field splitting effects as the cause for the paramagnetic admixtures in MMOH and complex **1**, we have checked whether the particular ligand environment of the HXTA complex yields unusual electronic features. Since diamagnetic Ga(III) is known to substitute isomorphously for Fe(III), we have prepared the analogous $\text{Fe}^{\text{III}}\text{Ga}^{\text{III}}$ HXTA complex, **2** (see Materials). For **2**, one can study the paramagnetic properties of the local Fe(III) site in the absence of interatomic exchange. Our preparation of $\text{Fe}^{\text{III}}\text{Ga}^{\text{III}}$ HXTA contained a mixture of $\text{Ga}^{\text{III}}\text{Ga}^{\text{III}}$, $\text{Fe}^{\text{III}}\text{Ga}^{\text{III}}$, and $\text{Fe}^{\text{III}}\text{Fe}^{\text{III}}$ dimers. Figure 5 shows a Mössbauer spectrum of a polycrystalline sample, recorded at 1.5 K in an applied field of 3.0 T; we have also studied spectra at 4.2 K in fields of 0.5, 1.0, 3.0, and 8.0 T. The central feature in the spectrum of Figure 5 (accounting for 2/3 of the total Fe) is contributed by complex **1** while the remainder belongs to the $\text{Fe}^{\text{III}}\text{Ga}^{\text{III}}$ dimer. We have also studied the EPR spectra (not shown) of a sample dissolved in $\text{CH}_3\text{CN}/\text{CH}_3\text{OH}$ (50:50 (v/v)). These spectra are typical of a high-spin ferric complex with $E/D = 0.30$; because E/D is near the rhombic limit the resonances of the ground and upper Kramers doublets overlap, leaving the sign of D undetermined. The solid line in Figure 5 is the result of spectral simulation for a monomeric high-spin ferric site based on eqs 1–5 for $J = d = D_{AB} = 0$, with site B absent. These simulations have revealed that the magnetic hyperfine tensor is isotropic to within 1%; $A_{x,y,z} = A_0 = -30.0 \pm 0.3$ MHz. Moreover, the zero-field splitting is small as expected, namely $D = 0.4$ cm^{-1} . These results suggest that there is nothing unusual about the intrinsic parameters (A_i , D_i) of the Fe(III) sites of complex **1**.

Because ΔE_Q is small for complex **1**, we can neglect the quadrupole interactions for the following arguments. The sample of Figure 2B was studied in an 8.0 T field that was applied parallel to the observed γ -radiation. For a strictly diamagnetic species the nuclear quantization axis would be parallel to the applied field for all ^{57}Fe nuclei in the sample. Under these conditions the nuclear $\Delta m = 0$ transitions are quenched; for a detailed discussion see ref 27. However, the two bands marked in Figure 2B occur precisely at Doppler velocities where nuclear $\Delta m = 0$ lines would occur. This observation shows that the paramagnetic admixtures into the $S = 0$ ground state of complex **1** produce internal magnetic fields with substantial components perpendicular to the direction of the applied field. In the spin Hamiltonian approximation the internal magnetic field can be written as $\mathbf{B}_{\text{int},i} = -\langle \mathbf{S}_i \rangle A_0 / g_n \beta_n$,

(26) Scaringe, R. P.; Hodgson, D. J.; Hatfield, W. E. *Mol. Phys.* **1978**, *35*, 701–713.

(27) Münck, E.; Huynh, B. H. In *ESR and NMR of Paramagnetic Species in Biological and Related Systems*; Bertini, I., Drago, R. S., Eds.; Reidel Publishing Company, Holland, 1979; pp 275–288.

Table 1. Mössbauer Parameters of $[\text{Fe}^{\text{III}}\text{Fe}^{\text{III}}(\text{HXTA})(\text{O}_2\text{CCH}_3)_2]^-$, Complex **1**, and $[\text{Ga}^{\text{III}}\text{Fe}^{\text{III}}(\text{HXTA})(\text{O}_2\text{CCH}_3)_2]^-$, Complex **2**

	δ (mm/s)	ΔE_Q (mm/s)	η	A_0 (MHz)	$D_A = D_B$ (cm^{-1})	E/D	d_z (cm^{-1})	J (cm^{-1})
1	0.48(1)	0.59(2)	0.4	-30.0 ^a	-0.7	0.3 ^a	2.2(7)	20(2)
2	0.49(4)	0.7(2)	0.8	-30.0(3)	0.4(2)	0.3		

^a A_0 value and $E/D = 0.3$ of complex **1** are those determined for **2**. Numbers in parentheses are estimated uncertainties in the least relevant digit.

with $i = \text{A, B}$, suggesting that we require an interaction that produces expectation values $\langle \mathbf{S}_i \rangle$ with components perpendicular to the applied field. Furthermore, a closer inspection of the spectrum of Figure 2B shows that the internal field has to combine with the applied field to produce an effective field at the ^{57}Fe nucleus with a magnitude larger than the applied field, and that this must occur for all molecular orientations. These considerations directed our attention to the $\mathbf{d} \cdot (\mathbf{S}_\text{A} \times \mathbf{S}_\text{B})$ term in eq 2. This term produces expectation values of the local spins perpendicular to the applied field, and thus can produce $\Delta m = 0$ lines as well as the desired effective magnetic fields.^{28,29}

We have written a computer program that calculates Mössbauer spectra by diagonalization of eqs 1–5. Since essentially all parameters in eqs 2 and 3, except $|\mathbf{d}|$, are known quite well, the problem of fitting the data is reduced to determining essentially one unknown from a series of high-field Mössbauer spectra taken at 1.5 and 4.2 K. (For temperatures above 10 K, the spectra suffer from relaxation effects and their features are unresolved.) Since mixing by the zero-field splitting terms is negligibly small (For $|D_A| = |D_B| = 0.7 \text{ cm}^{-1}$ and 8.0 T applied field, the magnetic hyperfine fields directly attributable to ZFS's are proportional to $(2D_A/3J)^2$ and are smaller than 0.4 T), the system, except for the antisymmetric exchange term, is essentially isotropic and therefore only the magnitude of \mathbf{d} matters. The sensitivity of the Mössbauer spectra to variations in $|\mathbf{d}|$ is illustrated by the theoretical spectra shown in Figure 6.

Figure 7 shows the results of our simulations for complex **1**, generated from eqs 1–5 with the parameters listed in Table 1. Overall, the theory fits the data very well. In particular, the splittings, the line shapes of the outermost features, and the intensities of the $\Delta m = 0$ lines are well represented. Thus, inclusion of the $\mathbf{d} \cdot (\mathbf{S}_\text{A} \times \mathbf{S}_\text{B})$ term produces, for $d_z = 2.2 \text{ cm}^{-1}$, all the desired features. We indicated above that the zero-field splitting terms of eq 2 decrease the magnetic hyperfine splittings (because mixing produces negative $\langle \mathbf{S}_\text{A} \rangle$ and $\langle \mathbf{S}_\text{B} \rangle$ at both iron sites). In the presence of the $\mathbf{d} \cdot (\mathbf{S}_\text{A} \times \mathbf{S}_\text{B})$ term, however, the zero-field splittings lead to increased magnetic splittings in our case. This phenomenon arises because the ZFS terms contribute to the splitting of the $S = 1$ multiplet, which is admixed in second order into the ground state by the $\mathbf{d} \cdot (\mathbf{S}_\text{A} \times \mathbf{S}_\text{B})$ term. Hence, the magnitude of the determined \mathbf{d} depends somewhat on the choice of the ZFS parameters and on the value of J . For the simulations shown in Figure 7, we have adjusted $D_A = D_B$ such that the shapes of the absorption bands are best reproduced. For the final simulation we have chosen $D_A = D_B = -0.7 \text{ cm}^{-1}$. This is somewhat higher than

the value obtained for the Fe(III) site of the $\text{Ga}^{\text{III}}\text{Fe}^{\text{III}}$ dimer, but the $D_A = D_B$ for complex **1** might contain a contribution from anisotropic exchange, D_{AB} .

The data of MMOH were more difficult to fit for various reasons. First, there is evidence from Mössbauer, EPR,¹ and EXAFS³¹ spectroscopy that *M. trichosporium* MMOH preparations are somewhat heterogeneous; typical preparations reveal the presence of at least two cluster forms, perhaps in variable proportions. Second, the two iron sites of the diferric cluster are inequivalent, and the quadrupole splittings are larger. Since there is no symmetry element, the number of unknowns is much larger. Moreover, the quadrupole tensors and zero-field splitting tensors can have different principal axis systems. To keep the number of unknowns at a manageable level, we have analyzed the data by assuming that $D_A = D_B$ and that the electric field gradient tensors of both sites have a common principal axis frame. We obtained the best results when the \mathbf{d} was directed along the y -axis of the quadrupole tensors. A d_y value of about 1.5 cm^{-1} was required to generate the theoretical spectra with a splitting that matches the outermost features of the MMOH experimental spectra. This value of d_y , however, did not produce the correct intensity of the (weak) $\Delta m = 0$ bands. This problem could be remedied by assuming the presence of a second diiron cluster, representing ca. 20% of Fe, having a diamagnetic ground state (such a state is achieved when the ratio $|\mathbf{d}|/J \approx 0$ for $J \geq 15 \text{ cm}^{-1}$). Interestingly, the fractions roughly agree with EXAFS studies of the diferric protein³¹ which have revealed the presence of two populations with 3.1 ($\approx 70\%$) and 3.4 Å ($\approx 30\%$) Fe–Fe separations. Moreover, EPR studies¹ of mixed-valent MMOH have indicated two species in similar concentration ratios. Given the large number of unknowns, the fitting parameters, quoted in the caption of Figure 8, should be viewed with caution. However, to match the observed magnetic splittings, the simulations require substantial antisymmetric exchange ($1 \text{ cm}^{-1} \leq d_y \leq 2.4 \text{ cm}^{-1}$ for $J = 15 \text{ cm}^{-1}$ and $D_A = D_B < 1 \text{ cm}^{-1}$).

Finally, we wish to comment on the magnetization data of complex **1** shown in Figure 3. The χ vs $1/T$ curves were obtained by diagonalization of eqs 2 and 3 and powder averaging. Our data analysis suggests that our sample contained two minor impurities, namely a monomeric paramagnetic species representing ca. 0.8% of the total Fe (assumed to be high-spin Fe^{2+} since the sample did not exhibit any EPR signal) and a ferromagnetic impurity (about 0.3% of total Fe if the contaminant were Fe^{3+}). The former can be recognized at low temperatures by the observation of nested magnetization curves that vary with temperature; its contribution is indicated separately in Figure 3. It is, of course, difficult to identify and characterize a 0.8% impurity; however, the Hamiltonian of eqs 2 and 3 does not produce the observed fanning of the low-temperature χ values for different fields. The presence of a minor ferromagnetic impurity is indicated by the observation that χ is field dependent at temperatures between 10 and 70 K.

(28) In our previous MMOH study¹ we have suggested that antisymmetric exchange is not responsible for the increased magnetic hyperfine splittings. Lack of spectral resolution of the MMOH spectra and insufficient insight into some of the spectroscopic consequences of the antisymmetric term contributed to that misjudgment.

(29) In principle, an \mathbf{A} tensor with antisymmetric components can give rise to hyperfine field components transverse to the applied field. But as our data on the $\text{Ga}^{\text{III}}\text{Fe}^{\text{III}}$ dimer show, the \mathbf{A} tensor of the ferric site is highly isotropic. Moreover, even if the \mathbf{A} tensor had antisymmetric components, the electronic ground state must have acquired by some additional unknown mechanism sizable expectation values $\langle \mathbf{S}_i \rangle$. For complexes containing low-spin ferric ions antisymmetric \mathbf{A} tensor components can be expected if the site symmetry is sufficiently low.³⁰

(30) Oosterhuis, W. T.; Lang, G. *Phys. Rev.* **1969**, *178*, 439–456.

(31) Shu, L.; Liu, Y.; Lipscomb, J. D.; Que, L., Jr. *J. Biol. Inorg. Chem.* **1996**, *1*, 297–304.

The assumed contributions of both contaminants are indicated separately in Figure 3.

The sensitivity of the magnetization curves to the $\mathbf{d} \cdot (\mathbf{S}_A \times \mathbf{S}_B)$ term is illustrated by the χ vs $1/T$ plot of Figure 9, which shows theoretical curves for $d_z = 2.2 \text{ cm}^{-1}$ and $d_z = 0$. It can be seen that the data would be most sensitive to $|\mathbf{d}|$ at temperatures where only the ground singlet is populated. Of course, magnetic impurities and uncertainties in the diamagnetic corrections would introduce large uncertainties for the analysis; such impurities have little effect, if any, for the analysis of the Mössbauer data.

Discussion

In the previous section we have presented the analysis of our data as obtained by computer diagonalization of eqs 1–5. To elucidate how the $\mathbf{d} \cdot (\mathbf{S}_1 \times \mathbf{S}_2)$ term affects the Mössbauer spectra and the magnetization data, it will be useful to discuss the electronic system in a perturbation treatment. Let us assume that the applied field is along z and that \mathbf{d} of eq 2 is in the x - z plane at an angle α with respect to the field. Neglecting zero-field splittings, eq 2 becomes

$$H = JS_A \cdot S_B + g_0 \beta B S_z + d \sin \alpha \{S_A \times S_B\}_x + d \cos \alpha \{S_A \times S_B\}_z \quad (7)$$

Assuming $|\mathbf{d}| = d \ll J$ and neglecting multiplets with $S > 1$, we restrict our attention to the $S = 0$ ground state, $|0,0\rangle$, and the $S = 1$ states, $|1,M\rangle$. The Hamiltonian matrix for the selected states then assumes the form:

	$ 1,1\rangle$	$ 1,0\rangle$	$ 1,-1\rangle$	$ 0,0\rangle$
$\langle 1,1 $	$J + \beta g_0 B$	0	0	$-\frac{i}{2} d \sin \alpha \sqrt{\frac{35}{6}}$
$\langle 1,0 $	0	J	0	$i d \cos \alpha \sqrt{\frac{35}{6}}$
$\langle 1,-1 $	0	0	$J - \beta g_0 B$	$\frac{i}{2} d \sin \alpha \sqrt{\frac{35}{6}}$
$\langle 0,0 $	h.c.	h.c.	h.c.	0

For the $S = 0$ ground state the perturbation treatment yields for the expectation values of the local spins, $\langle S_A \rangle$ and $\langle S_B \rangle$,

$$\begin{aligned} \langle S_{A,x} \rangle &= \langle S_{B,x} \rangle = 0 \\ \langle S_{A,y} \rangle &= -\langle S_{B,y} \rangle = -\frac{35}{6} d \sin \alpha \frac{g_0 \beta B}{J^2 - (g_0 \beta B)^2} \quad (8) \\ \langle S_{A,z} \rangle &= \langle S_{B,z} \rangle \propto \frac{\beta B d^2}{J^3} \end{aligned}$$

Because $\langle S_A \rangle + \langle S_B \rangle = \langle S \rangle$, the expectation values of the total spin in the direction perpendicular to the applied field are zero. The induced hyperfine fields, $H_{\text{int},A} = -H_{\text{int},B} = -\langle S_{A,B,y} \rangle A_0 / g_n \beta_n$, are perpendicular to the plane containing \mathbf{d} and \mathbf{B} . For $g_0 \beta B \ll J$, the hyperfine fields are linear in B . This linear field dependence arises from the Zeeman splitting of the $S = 1$ multiplet through the energy denominators $(J - g_0 \beta B)^{-1}$ and $(J + g_0 \beta B)^{-1}$, which combine to yield the $\langle S_{i,y} \rangle$ values of eq 8. Because $B_{\text{int},z}$ is small compared to $B_{\text{int},y}$, the internal field is perpendicular to the applied field, and thus the effective field sensed by the ^{57}Fe nucleus, $B_{\text{eff}} = [(B + B_{\text{int},z})^2 + B_{\text{int},y}^2]^{1/2} \cong [B^2 + B_{\text{int},y}^2]^{1/2}$, is larger than B for all molecules in the sample (for complex **1**, $B_{\text{int},y} = 4.9 \text{ T}$ for $\alpha = 90^\circ$ and $B_{\text{int},z} = 0.4 \text{ T}$ at

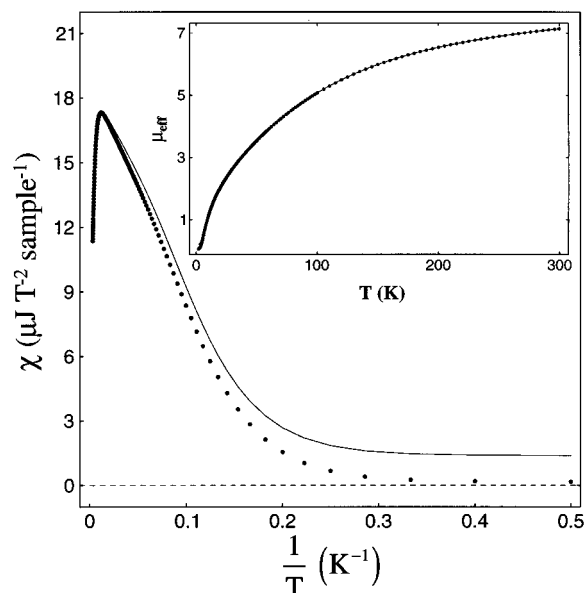


Figure 9. Calculated magnetization curves for $B = 5.0 \text{ T}$ illustrating the effect of the $\mathbf{d} \cdot (\mathbf{S}_A \times \mathbf{S}_B)$ term. Curves were computed for complex **1** from the parameters in Table 1 for $d_z = 0$ (full circles) and $d_z = 2.2 \text{ cm}^{-1}$ (solid line). All other relevant parameters are listed in Table 1. The inset depicts μ_{eff} vs T .

$B = 8.0 \text{ T}$). This accounts for the increased splitting observed in the spectra of Figures 2A and 2B. Because the internal field is at right angles to the applied field and because $B_{\text{int},A} = -B_{\text{int},B}$, one cannot determine the sign of \mathbf{d} from the Mössbauer spectra.

In general, the intensity of nuclear $\Delta m = 0$ lines is proportional to $\sin^2 \theta$, where θ is the angle between the nuclear quantization axis and the propagation direction of the observed $14.4 \text{ keV } \gamma$ -rays. For $\mathbf{d} = 0$ and \mathbf{B} parallel to the observed γ -rays, $\theta = 0$. In the presence of antisymmetric exchange, we have $\sin \theta = |B_{\text{int}}/B_{\text{eff}}| \approx 0.5$ and consequently nuclear $\Delta m = 0$ lines are observed in the spectra of complex **1**.

The SQUID magnetometer used in this study senses the component of the magnetization that is parallel to the applied field. As can be seen from the above expressions, the contribution of the antisymmetric term to the parallel magnetization is very small. For temperatures for which population of the $S = 1$ manifold is negligible we can derive, by powder-averaging the susceptibility, the paramagnetic contribution due to the antisymmetric term as

$$\chi_{\text{ave}} = N_A \frac{35\pi\beta^2 g_0^2}{24} \left(\frac{d^2}{J^3} \right) \quad (9)$$

From this expression we estimate for $J = 20 \text{ cm}^{-1}$ and $d = 2.2 \text{ cm}^{-1}$ that $\chi_{\text{ave}} = 1.55 \mu\text{J T}^{-2} \text{ sample}^{-1}$. This agrees to within 12% with our experimental value of $1.38 \mu\text{J T}^{-2} \text{ sample}^{-1}$.

As pointed out in the Introduction, we have been intrigued by the observation of increased magnetic splittings in the low-temperature Mössbauer spectra of MMOH and complex **1**. With the exception of the $\mathbf{d} \cdot (\mathbf{S}_A \times \mathbf{S}_B)$ term, we have been able to eliminate all other terms of eqs 2 and 3 as a cause for this peculiar behavior. Although there are as yet no reports in the literature on high-spin $\text{Fe}^{\text{II}}\text{Fe}^{\text{II}}$ or low-spin $\text{Fe}^{\text{III}}\text{Fe}^{\text{III}}$ dimers, we would not have been surprised to observe evidence for the $\mathbf{d} \cdot (\mathbf{S}_A \times \mathbf{S}_B)$ term for these systems. The ground states of these systems, in particular the ground states of dimers involving low-spin $\text{Fe}(\text{III})$ (see ref 12), have substantial unquenched orbital angular momentum, and thus one would expect from Moriya's

order of magnitude estimate, $d \cong (\Delta g/g)J'$, that the antisymmetric term can be observed under favorable experimental conditions. For the low-spin $\text{Fe}^{\text{II}}\text{Fe}^{\text{III}}$ and high-spin $\text{Fe}^{\text{II}}\text{Fe}^{\text{II}}$ dimers, as well as for the Cr(III) and Cu(II) complexes mentioned in the Introduction, the ground and excited states under consideration belong to the same (L,S) manifold; for such systems Moriya has explained the microscopic origin of the $\mathbf{d} \cdot (\mathbf{S}_A \times \mathbf{S}_B)$ term. The situation is, however, quite obscure for high-spin $\text{Fe}^{\text{III}}\text{Fe}^{\text{III}}$ dimers. The high-spin ferric ion has no excited states with $S = 5/2$ and thus one would have to construct an effective dimer Hamiltonian for the ground manifold that reflects admixtures from excited quartet states; because the ground manifold would contain $S = 3/2$ admixtures, \mathbf{S}_A and \mathbf{S}_B of the $\mathbf{d} \cdot (\mathbf{S}_A \times \mathbf{S}_B)$ term would become fictitious spins. We are not aware of theoretical studies that address this problem.

Conclusions

We have found here that the dinuclear clusters of complex **1** and MMOH exhibit substantial antisymmetric exchange, namely $d \approx 1.5 \text{ cm}^{-1}$ for MMOH and $d = 2.2 \pm 0.7 \text{ cm}^{-1}$ for complex

1. These values compare well with $d = 1.4 \text{ cm}^{-1}$ reported²⁰ for the trinuclear ferric complex $[\text{Fe}_3\text{O}(\text{O}_2\text{CCH}_3)_6(\text{H}_2\text{O})_3]\text{Cl} \cdot 5\text{H}_2\text{O}$. Our d value for complex **1** should be quite reliable because all other parameters that enter the analysis were well-known and have values favorable to our studies, i.e., the Fe sites are equivalent, quadrupole and zero-field splittings are small, and the Zeeman terms are highly isotropic. The present study shows that Mössbauer spectroscopy can be exquisitely sensitive to the antisymmetric exchange term (see Figure 6). It would be interesting to confirm that the \mathbf{d} vector of complex **1** is perpendicular to the 2-fold axis as required by the symmetry rules of Moriya.¹⁵ Such information could be furnished by high-field Mössbauer studies of monocrystals, provided that crystals of sufficient size can be obtained for complex **1**. Such studies are under consideration.

Acknowledgment. This work was supported National Institutes of Health grants GM-22701 (to E.M.), GM-38767 (to L.Q.), and GM-40466 (J.D.L.).

JA981065T